Vector-Field-Orientation Tracking Control for a Mobile Vehicle Disturbed by the Skid-Slip Phenomena

Maciej Michałek*, Piotr Dutkiewicz
Marcin Kiełczewski, Dariusz Pazderski

Abstract

The paper is devoted to the trajectory tracking control task for a differentially-driven vehicle moving on a plane surface under conditions of the persistent skid-slip phenomena. The Vector Field(s) Orientation (VFO) control strategy, presented originally for undisturbed case in [6], has been reformulated here to the new disturbed motion conditions. The extension of the VFO strategy relies on introduction of the nonlinear skid-slip influence compensator in the feed-forward loop, which in practical implementation involves the real-time estimation of the skid-slip velocities and their time-derivatives. The approach considers the skid-slip effects solely on the kinematic level avoiding the need of modeling a complicated phenomenon of the wheels-ground interaction. Theoretical analysis shows the asymptotic tracking ability for the position trajectory with boundedness of the orientation error. Experimental results included in the paper reveal substantial tracking quality improvement resulting from the utilization of the proposed skid-slip influence compensator.

1 Introduction

Appearance of skid and slip phenomena in practice of vehicle motion control is equivalent to violation of nonholonomic constraints, which in turn usually determine the *nominal* kinematic models used for description of restricted-mobility wheeled robots. If skid-slip effects are negligibly small, they can be omitted in system modeling. It is justified when sufficiently slow motion with low acceleration and with good wheel-ground contact conditions can be assumed. In such circumstances the possible skid-slip effects can be treated as an occasional, temporal and vanishing system disturbance, which usually can be effectively attenuated by properly designed motion feedback controller. However in some particular real-life motion tasks the skid-slip phenomena can persistently influence the system in such a degree that exclusion of them in a system model leads to significant control performance deterioration and the motion safety decreasing. Moreover, in particular motion tasks it is usually impossible or undesirable to avoid or attenuate the skid and slip. Hence, the control problem is to preserve the desired motion performance in spite of the skid-slip presence by attenuation of its negative influence on the overall control quality. Robustness improvement of automated motion control in the presence of skid-slip phenomena usually involves inclusion and utilization of some skid-slip model in a control law design. In the literature of the robotics community there are not many works explicitly related to the problem of control in skid-slip conditions (one can recall [2, 4, 8, 9, 14, 16, 17]). Much less attention has been paid on practical validation of

*Corresponding author. All authors are with Chair of Control and Systems Engineering, Poznań University of Technology, Piotrowo 3a, 60-965 Poznań, Poland.

the presented solutions – see for example [3, 8, 13, 18].
Skid and slip are the intrinsic phenomena necessary for proper operation (also in a case of slow motion) of an important class of so-called Skid-Steering Wheeled Mobile Robots (SSWMRs). For this class of underactuated systems the set of feasible accelerations is restricted and their dynamics are not integrable [11]. Mathematical modeling of SSWMRs often results from a simplifying assumption where the lateral dynamics of a vehicle is neglected. The attention is mainly focused on the longitudinal dynamics considering the slip phenomenon based on its physical or empirical model [12, 21, 22]. It is worth noting that on a kinematic level the SSWMRs are commonly modeled as a perturbed unicycle-like system. Thus the control solutions dedicated for the latter can be, at least in some reasonable conditions, practically applicable also for SSWMRs, [15, 17, 18].

In existing works authors usually use one of the following skid-slip modeling and control design approaches: dynamic-like one [16], kinematic-like one [2, 4, 13, 14, 17] or combined approach as in [9]. Dynamic-like modeling of skid-slip effects involves considering the sophisticated or not fully recognized problems like wheel-ground contact or tire-ground friction phenomena. These complications usually lead to practical limitations of the approach. Alternative and simpler way of skid/slip-influence modeling comes from the kinematic approach, where skid and slip influence is represented as additional velocity terms in a system model. Such an approach seems to be practically attractive and justified, since the velocity disturbance is always a direct consequence of the skid-slip phenomena regardless of their any physical reasons. The latter approach to skid-slip treatment will be used in the sequel of this paper due to its methodological simplicity.

Presented work provides an extension and experimental validation of the Vector Field(s) Orientation (VFO) control strategy adopted to the case of persistently disturbed motion conditions, [5]. The attention will be paid on the position-trajectory tracking task in the presence of persistent but bounded kinematic disturbances originated from the skid and slip effects. The control concept utilizes geometrical features of the disturbed kinematic model of the differentially driven vehicle (DDV). The idea presented in this paper is an application extension of the *nominal* VFO controller (described in [6]) adopted here to the new motion conditions. Proposed modification relies on introduction of the nonlinear skid/slip-influence compensator realized in a feed-forward loop using a vision feedback and the Kalman filter idea for practical estimation of the skid-slip components and their time-derivatives. Experimental results obtained in the laboratory conditions reveal the possibility of effective robot motion control in spite of the partial lost of the wheels-ground adhesion.

2 System model and problem statement

2.1 Nominal and disturbed vehicle model

Let us consider the nominal (non-disturbed) kinematic model of a differentially driven mobile vehicle:

$$\begin{bmatrix}\dot{\theta}\\ \dot{x}\\ \dot{y}\end{bmatrix} = \begin{bmatrix}1 & 0\\ 0 & \cos\theta\\ 0 & \sin\theta\end{bmatrix}\begin{bmatrix}u_1\\ u_2\end{bmatrix} \quad \Rightarrow \quad \dot{\boldsymbol{q}} = \boldsymbol{G}(\boldsymbol{q})\boldsymbol{u}, \tag{1}$$

where $\boldsymbol{q} = [\theta\ x\ y]^T \in \mathbb{R}^3$ is a state vector describing the orientation angle and the position coordinates of the vehicle in a global frame, respectively (see Fig. 1). Nominal control inputs $[u_1\ u_2]^T = \boldsymbol{u} \in \mathbb{R}^2$ have the physical interpretation of angular and driving

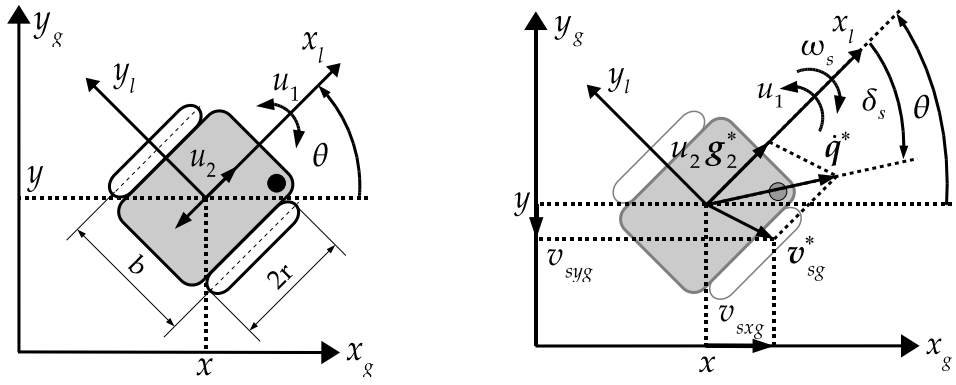

Figure 1: Differentially driven vehicle in a global frame (left) and in the presence of skid-slip phenomena (right)

velocity, respectively which in the case of a DDV can be realized according to the well known relation

$$\begin{bmatrix} u_1 \\ u_2 \end{bmatrix} = \begin{bmatrix} r/b & -r/b \\ r/2 & r/2 \end{bmatrix} \begin{bmatrix} \omega_R \\ \omega_L \end{bmatrix} \quad \Rightarrow \quad \boldsymbol{u} = \boldsymbol{J}\boldsymbol{\omega} \tag{2}$$

with a Jacobian matrix $\boldsymbol{J}$ (as a function of a wheel radius r and a wheel base b denoted in Fig. 1) and angular velocities of the right ω_R and left ω_L vehicle wheels, respectively. The nominal model (1)-(2) assumes that the overall resultant angular and longitudinal vehicle body velocities (denoted here as u_1 and u_2) result directly and only from the action of wheels driven by motors. It is so called *rolling-without-skidding/slipping* motion condition. The non-skidding motion means the absence of a lateral velocity component (as expressed in a local body frame) and is defined by the following nonholonomic constraint:

$$\boldsymbol{A}^T(\boldsymbol{q})\dot{\boldsymbol{q}} = 0, \quad \text{where} \quad \boldsymbol{A}^T(\boldsymbol{q}) = \begin{bmatrix} 0 & -\sin\theta & \cos\theta \end{bmatrix}. \tag{3}$$

The non-slipping assumption means in turn that the overall longitudinal velocity of the unicycle results directly and only from the angular velocity of the wheel. Let us now introduce a skid-slip model, which implies violation of the *rolling-without-skidding/slipping* assumption. According to the postulated strict kinematic approach, the skid-slip phenomena can be taken into account in the model (1) with an additional resultant *skid-slip velocity* $\boldsymbol{v}_{sg}$:

$$\begin{bmatrix} \dot{\theta} \\ \dot{x} \\ \dot{y} \end{bmatrix} = \begin{bmatrix} 1 & 0 \\ 0 & \cos\theta \\ 0 & \sin\theta \end{bmatrix} \begin{bmatrix} u_1 \\ u_2 \end{bmatrix} + \begin{bmatrix} \omega_s \\ v_{sxg} \\ v_{syg} \end{bmatrix} \tag{4}$$

where $[\omega_s \ \boldsymbol{v}_{sg}^{*T}]^T \triangleq \boldsymbol{v}_{sg} \in \mathbb{R}^3$ and $\boldsymbol{v}_{sg}^* \triangleq [v_{sxg} \ v_{syg}]^T \in \mathbb{R}^2$ are expressed in a global frame (see fig. 1). Mapping the disturbance $\boldsymbol{v}_{sg}$ into a local frame attached to the vehicle body one can equivalently write:

$$\begin{bmatrix} \dot{\theta} \\ \dot{x} \\ \dot{y} \end{bmatrix} = \begin{bmatrix} 1 \\ 0 \\ 0 \end{bmatrix} (u_1 + \omega_s) + \begin{bmatrix} 0 \\ \cos\theta \\ \sin\theta \end{bmatrix} (u_2 + v_{sx}) + \begin{bmatrix} 0 \\ -\sin\theta \\ \cos\theta \end{bmatrix} v_{sy}, \tag{5}$$

where the terms ω_s, v_{sx} and v_{sy} are the skid-slip velocity components defined in a local frame: $[\omega_s \ v_{sx} \ v_{sy}]^T \triangleq \boldsymbol{v}_s \in \mathbb{R}^3$. Following the recent work [20] and analyzing the perturbed model (5) one can distinguish two kinds of disturbances: 1) *input-additive* ones like ω_s and v_{sx} related to the *slip* effect and 2) *unmatched* one equal to $\boldsymbol{A}(\boldsymbol{q})v_{sy}$,

which is a direct consequence of the *skid* phenomenon. Now, the signals u_1 and u_2 can be treated only as control inputs, which reflect physical impact of motor drives. It is worth to note, that additional velocity components ω_s, v_{sx} and v_{sy} included in (5) can represent all possible kinematic disturbances resulting either from skid-slip phenomena or from other effects not taken into account in the simplistic model like dynamics of vehicle body and motor drives. These additional contributions can be treated here as the *virtual skid-slip* elements. Hereafter we will understand the overall influence of the skid-slip in such a manner.

Since both types of disturbances (skid and slip) can be included in model (5) and since (2) is an invertible linear algebraic map, our further considerations will be related to the simpler unicycle model represented by (1) with control inputs u_1 and u_2.

2.2 Control problem formulation

The motion task for a vehicle is given by the admissible and persistently exciting reference trajectory $\boldsymbol{q}_t(\tau) = [\theta_t(\tau)\ x_t(\tau)\ y_t(\tau)]^T \in \mathbb{R}^3$ defined as a time-integral of the nominal model (1) for some bounded reference inputs $u_{1t}(\tau), u_{2t}(\tau) \in \mathbb{R}$ and for a given initial condition $\boldsymbol{q}_t(0)$. As a persistent excitation condition we understand the following relation:

$$\forall_{\tau \geqslant 0}\ u_{2t}(\tau) \neq 0, \tag{6}$$

which means that the reference vehicle is always in the translational motion. From now on we also assume that the skid-slip components in the disturbed model (4) or (5) are measurable (or can be practically estimated) and they together with the so-called *slip angle* δ_s (see Fig. 1) are bounded:

$$\omega_s(\tau),\ v_{sxg}(\tau),\ v_{syg}(\tau) \in \mathcal{L}_\infty, \qquad |\delta_s| < \pi/2. \tag{7}$$

The above assumption allows preserving the vehicle point-controllability (controllability of the vehicle position) as has been stated in [20]. We additionally assume that the lateral and longitudinal skid-slip components are continuous functions of time:

$$\dot{v}_{sxg}(\tau), \dot{v}_{syg}(\tau) \in \mathcal{L}_\infty. \tag{8}$$

Keeping up the above one can formulate the following control problem.

Problem 1 (Control problem) *For a given admissible reference trajectory $\boldsymbol{q}_t(\tau) \in \mathbb{R}^3$ which meets the persistent excitation condition (6) find a bounded feedback control law $\boldsymbol{u}(\boldsymbol{q}_t, \boldsymbol{q}, \cdot)$ for the disturbed model (4), which in the presence of bounded and continuous skid-slip phenomena guarantees boundedness of the orientation error e_θ and asymptotic convergence of the position error $\boldsymbol{e}^* = [e_x\ e_y]^T \in \mathbb{R}^2$ to zero: $\lim_{\tau\to\infty} \boldsymbol{e}^*(\tau) = \boldsymbol{0}$, where:*

$$e_\theta(\tau) \stackrel{\Delta}{=} \theta_t(\tau) - \theta(\tau)\ \in \mathbb{R}, \tag{9}$$

$$\boldsymbol{e}^*(\tau) = \begin{bmatrix} e_x(\tau) \\ e_y(\tau) \end{bmatrix} \stackrel{\Delta}{=} \begin{bmatrix} x_t(\tau) - x(\tau) \\ y_t(\tau) - y(\tau) \end{bmatrix}\ \in \mathbb{R}^2. \tag{10}$$

Remark 1 *Boundedness of the orientation error e_θ prevents the situation where the vehicle persistently turns around the vertical axis and simultaneously tracks the position trajectory $\boldsymbol{q}_t^* = [x_t\ y_t]^T$. Such a solution seems to be undesirable in practice. It is worth to stress, that asymptotic convergence of the whole tracking error $\boldsymbol{e} = [e_\theta\ e_x\ e_y]^T$ to zero in the presence of persistent skid influence is not possible as has been stated in [20] (in this case the vehicle loses its* posture controllability*) what is intuitively understood.*

3 VFO control strategy

VFO controller with skid-slip compensation[1], which will be proposed in the sequel, originates from the nominal VFO concept designed for the case of *rolling-without-skidding/slipping* assumption. Therefore, it seems desirable to recall basic ideas of the VFO methodology to make our further considerations more clear. Due to practical reasons the following description will be shortened only to principles. More details can be found in [6].

3.1 Principles of the VFO control

The VFO control design methodology and control strategy result from simple geometrical interpretations of a system model structure and has been applied so far to several examples of nonholonomic driftless systems with two inputs[2]. System (1) is an archetypical example of the VFO concept utilization. Principles of the method result from possible decomposition of the model (1) into two subsystems:

$$\Sigma_\theta: \quad \dot{\theta} = u_1, \qquad \Sigma^*: \quad \dot{\boldsymbol{q}}^* = \boldsymbol{g}_2^*(\theta)u_2,$$

where $\boldsymbol{q}^* = [x\ y]^T$ and $\boldsymbol{g}_2^*(\theta) = [\cos\theta\ \sin\theta]^T$. Using simple geometrical interpretation explained in the sequel Σ_θ is called the *orienting subsystem* and Σ^* – the *pushing subsystem*. Since the direction (and orientation) of vector $\boldsymbol{g}_2^*(\theta)$ in $\mathbb{R}^2$ (and consequently of velocity $\dot{\boldsymbol{q}}^*$ in $\mathbb{R}^2$) depends on θ variable, it has been proposed to call θ the *orienting variable*, and the u_1 input – the *orienting control*. Following this interpretation u_2 is the *pushing control*, since it *pushes* the sub-state $\boldsymbol{q}^*$ along the current direction of $\boldsymbol{g}_2^*(\theta)$ (compare structure of Σ^*). The original VFO control law for a tracking task can be derived according to the demand of perfect matching between the velocity vector $\dot{\boldsymbol{q}}$ of the model (1) and the introduced and particularly designed *convergence vector field* $\boldsymbol{h} = [h_1\ \boldsymbol{h}^{*T}]^T \in \mathbb{R}^3$. The vector[3] $\boldsymbol{h}(\boldsymbol{q}, \boldsymbol{q}_t, \cdot)$ defines at every point $\boldsymbol{q}$ in the vehicle state space an instantaneous convergence direction to a reference trajectory $\boldsymbol{q}_t(\tau)$. Its definition stays a degree of freedom for the designer, since it can be determined in several ways. In the VFO strategy the way in which $\boldsymbol{h}(\boldsymbol{q}, \boldsymbol{q}_t, \cdot)$ defines the convergence direction is especially important and crucial for the motion quality obtained in the resultant VFO closed-loop system. Namely, using the nonholonomic nature of the system (1) the simultaneous attenuation of both the position and the orientation errors during a transient stage implies highly oscillatory vehicle movement, which usually cannot be accepted in practical implementations. To avoid the transient oscillations the first component of $\boldsymbol{h}$ can be designed with relation to introduced the so called *auxiliary orienting variable* $\theta_a(\tau) = \arg(\boldsymbol{h}^*(\tau))$[4] rather than to the reference angle $\theta_t(\tau)$. The auxiliary variable $\theta_a(\tau)$ allows the vehicle smoothly approach a position trajectory $\boldsymbol{q}_t^*(\tau) = [x_t(\tau)\ y_t(\tau)]^T \in \mathbb{R}^2$ making only subsequently the vehicle orientation converge to the reference signal $\theta_t(\tau)$ (when the vehicle approaches a neighborhood of $\boldsymbol{q}_t^*$). Believing that there exist many possible constructions of the convergence vector field which fulfill mentioned conditions,

[1] For the sake of simplicity we will use the expression *skid-slip compensation* instead of *skid-slip influence compensation* which is in fact more strict in the sense of presented solution.

[2] Authors believe that the VFO method can be treated as a generalization of the polar-coordinates-like control concept.

[3] We will use hereafter the general notion, consistent with notion in [6], where $(\cdot)$ denotes all the so far undetermined arguments of a function.

[4] For the forward motion $\theta_a(\tau) := \arg(\boldsymbol{h}^*(\tau))$; for the backward motion $\theta_a(\tau) := \arg(\boldsymbol{h}^*(\tau)) \pm \pi$, see [6].

we have originally proposed the simple one coming from weighted linear combinations of particular errors and feed-forward velocity terms:

$$h_1 = k_1(\theta_a - \theta) + \dot{\theta}_a, \qquad \boldsymbol{h}^* = k_p(\boldsymbol{q}_t^* - \boldsymbol{q}^*) + \dot{\boldsymbol{q}}_t^*,$$

where $k_1, k_p > 0$ are the only two VFO controller parameters (they are very easily tunable). Combining mentioned geometrical interpretations related to the model (1) together with the concept of the convergence vector field the VFO control strategy can be described as follows. Let us partition the tracking control problem into two subtasks: 1) the *orienting subprocess*, where the orienting input u_1 is responsible for putting the direction of $\boldsymbol{g}_2^*(\theta)$ (and in a consequence direction of $\dot{\boldsymbol{q}}^*$) onto the direction defined by $\boldsymbol{h}^*(\boldsymbol{q}, \boldsymbol{q}_t, \cdot)$, and 2) the *pushing subprocess* where the pushing input u_2 is responsible for pushing the state $\boldsymbol{q}^*$ along $\boldsymbol{g}_2^*(\theta)$ toward the reference position trajectory $\boldsymbol{q}_t^*(\tau)$. Designing u_1 and u_2 in a way which allows accomplishing the above subtasks leads to the VFO control law. It will guarantee that the vehicle position $\boldsymbol{q}^*(\tau)$ will be converging toward $\boldsymbol{q}_t^*(\tau)$. However, since the orienting variable θ plays an auxiliary role during the orienting subprocess, only a proper construction of the $\boldsymbol{h}$ vector field will guarantee the terminal convergence of $\theta(\tau)$ to its reference $\theta_t(\tau)$ (the proposition for $\boldsymbol{h}$ vector field given above satisfies this condition). It is worth to note that the partition of the control process proposed above is especially natural for kinematics (1) and resembles the polar-coordinates-like control. It surprisingly (due to the more general treatment) can be successfully applied also to other kinematics like the nonholonomic manipulator or the chained system.

Additional heuristic concept used in the VFO control methodology is an idea of the *careful pushing*, which relies on making the pushing intensity (understood as $|u_2|$) proportional to the instantaneous orthogonal projection of $\boldsymbol{h}^*$ onto the current direction of the vehicle motion (determined by $\boldsymbol{g}_2^*(\theta)$). As a consequence, the *careful pushing* strategy admits the maximal pushing only for perfect direction matching between $\boldsymbol{g}_2^*(\theta)$ and convergence vector $\boldsymbol{h}^*(\boldsymbol{q}, \boldsymbol{q}_t, \cdot)$.

Utilization of the above principles will be clearly exemplified in the next subsection during presentation of our main result of this paper. The original (nominal) VFO control proposed in [6] assumed the following control input definitions: $u_1 = h_1$ and $u_2 = \| \boldsymbol{h}^* \| \cos\alpha \equiv \boldsymbol{g}_2^{*T}(\theta)\boldsymbol{h}^*$, where $\alpha = \angle(\boldsymbol{g}_2^*(\theta), \boldsymbol{h}^*)$. It will be shown that after necessary modifications related to the skid-slip phenomena, the VFO control law can be designed for the considered disturbed case in a similar way as for the nominal one. The nominal VFO control approach for the trajectory tracking task can be retrieved from Fig. 2 taking $\boldsymbol{v}_{sg}^* = \boldsymbol{0}$ and consequently: $\boldsymbol{H}^* = \boldsymbol{h}^*$ and $\dot{\boldsymbol{q}}^* = \boldsymbol{g}_2^* u_2$.

The above recall will clarify and justify particular selections made in the sequel.

3.2 VFO tracking control with skid-slip compensation

Let us define, according to considerations from Subsection 3.1, the positional component of the convergence vector field as follows:

$$\boldsymbol{h}^* = \begin{bmatrix} h_2 \\ h_3 \end{bmatrix} \triangleq k_p\, \boldsymbol{e}^* + \dot{\boldsymbol{q}}_t^*, \quad k_p > 0, \qquad \dot{\boldsymbol{q}}_t^* = \begin{bmatrix} \dot{x}_t \\ \dot{y}_t \end{bmatrix}, \tag{11}$$

where k_p is a design parameter. Definition (11) ensures that $\boldsymbol{h}^*$ for $\boldsymbol{e}^* \neq \boldsymbol{0}$ always points toward the positional reference trajectory $\boldsymbol{q}_t^*$ using simultaneously some kind of motion prediction along $\boldsymbol{q}_t^*$ by utilizing the feed-forward velocity term $\dot{\boldsymbol{q}}_t^*$. Since for the current tracking error $\boldsymbol{e}^* = \boldsymbol{q}_t^* - \boldsymbol{q}^*$ the vector $\boldsymbol{h}^*(\boldsymbol{e}^*, \dot{\boldsymbol{q}}_t^*)$ defines a desired direction for the

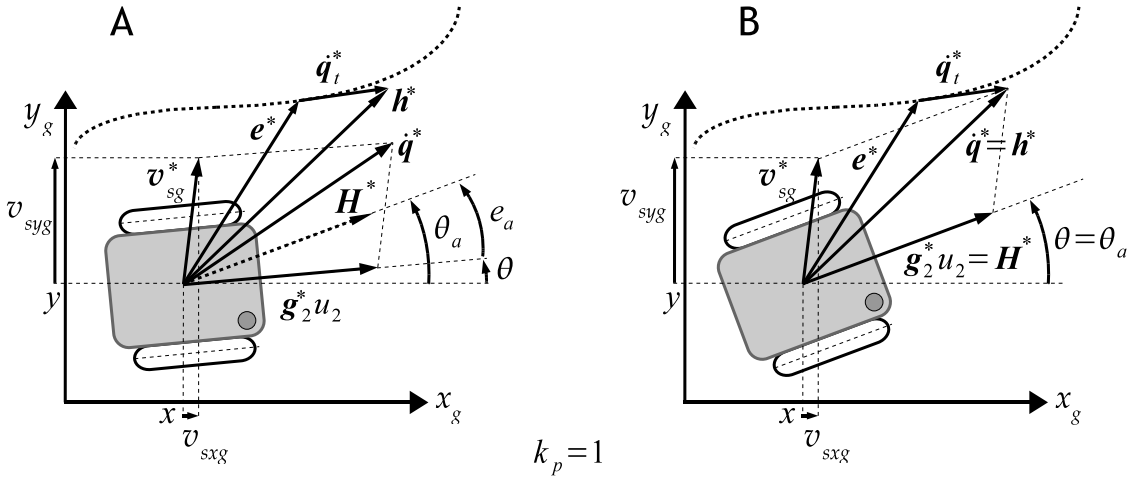

Figure 2: VFO control strategy with the skid-slip influence compensation in two cases: when $\dot{\boldsymbol{q}}^* \neq \boldsymbol{h}^*$ (A-left) and for $\dot{\boldsymbol{q}}^* = \boldsymbol{h}^*$ (B-right)

resultant vehicle motion, it is desirable to make the generalized velocity $\dot{\boldsymbol{q}}^*$ converge to $\boldsymbol{h}^*$, at least at the limit, as follows:

$$\lim_{\tau \to \infty} [\dot{\boldsymbol{q}}^*(\tau) - \boldsymbol{h}^*(\boldsymbol{e}^*(\tau), \dot{\boldsymbol{q}}_t^*(\tau))] = \boldsymbol{0}. \tag{12}$$

The above relation means that one expects matching of the orientations (directions) as well as of the norms for both vectors[5] $\dot{\boldsymbol{q}}^*$ and $\boldsymbol{h}^*$. Substituting particular terms from (4) and (11) into (12) gives the following condition

$$\lim_{\tau \to \infty} \begin{cases} u_2(\tau)\cos\theta(\tau) + v_{sxg}(\tau) - h_2(\tau) = 0 \\ u_2(\tau)\sin\theta(\tau) + v_{syg}(\tau) - h_3(\tau) = 0 \end{cases},$$

which can be rewritten in a more compact form as

$$\lim_{\tau \to \infty} [\mathrm{Atan2}\,(H_3\,\mathrm{sgn}(u_2), H_2\,\mathrm{sgn}(u_2)) - \theta(\tau)] = 0 \tag{13}$$

with

$$\boldsymbol{H}^* = \begin{bmatrix} H_2 \\ H_3 \end{bmatrix} \triangleq \boldsymbol{h}^* - \boldsymbol{v}_{sg}^* = \begin{bmatrix} h_2 - v_{sxg} \\ h_3 - v_{syg} \end{bmatrix}. \tag{14}$$

The limit (13) describes the so-called *orienting condition* (according to terminology introduced in [6]). Meeting (13) guarantees matching for orientations of vectors $\dot{\boldsymbol{q}}^*$ and $\boldsymbol{h}^*$ – matching for their norms will be considered in the sequel. To meet (13) let us introduce the auxiliary variable

$$\theta_a \triangleq \mathrm{Atan2c}\,(H_3\,\mathrm{sgn}(u_{2t}), H_2\,\mathrm{sgn}(u_{2t})) \in \mathbb{R}, \tag{15}$$

where $\mathrm{Atan2c}\,(\cdot,\cdot) : \mathbb{R}\times\mathbb{R} \mapsto \mathbb{R}$ is a continuous version[6] of $\mathrm{Atan2}\,(\cdot,\cdot) : \mathbb{R}\times\mathbb{R} \mapsto (-\pi, \pi]$. Note that in (15) we replaced u_2 term with the reference one u_{2t} due to the two reasons: to avoid possible chattering effect in control (note that according to assumption (6) the

[5]Note, that for $\boldsymbol{e}^* = \boldsymbol{0}$ the relation (12) implies: $\dot{\boldsymbol{q}}^*(\tau) - \dot{\boldsymbol{q}}_t^*(\tau) = \boldsymbol{0}$.

[6]Continuous-time computations of (13) is equivalent to time-integration of the velocity signal $\dot{\theta}_a(\tau)$ given by (18).

sign of $u_{2t}(\tau)$ is constant for all $\tau \geqslant 0$) and to guarantee proper transient behavior of a closed-loop system. If we now introduce the auxiliary error

$$e_a \stackrel{\Delta}{=} \theta_a - \theta, \qquad e_a \in \mathbb{R} \tag{16}$$

fulfillment of the orienting condition (13) involves simply making (16) converge to zero. Since the first component of $\boldsymbol{h}$ should define the convergence *direction* for the first state variable we propose to define it as follows:

$$h_1 \stackrel{\Delta}{=} k_1 e_a + \dot{\theta}_a, \qquad k_1 > 0, \tag{17}$$

where k_1 is a second design parameter, and

$$\dot{\theta}_a = \frac{\dot{H}_3 H_2 - H_3 \dot{H}_2}{\| \boldsymbol{H}^* \|^2}, \qquad \| \boldsymbol{H}^* \| \neq 0 \tag{18}$$

is a feed-forward velocity term (coming from the time-differentiation of (15)), where

$$\dot{H}_2 = k_p(\dot{x}_t - \dot{x}) + \ddot{x}_t - \dot{v}_{sxg}, \tag{19}$$

$$\dot{H}_3 = k_p(\dot{y}_t - \dot{y}) + \ddot{y}_t - \dot{v}_{syg}. \tag{20}$$

Using principles of the VFO method described in Subsection 3.1 we are ready to propose the VFO feedback control law considering the skid-slip disturbances as follows:

$$u_1 \stackrel{\Delta}{=} h_1 - \omega_s \quad \Rightarrow \quad u_1 = k_1 e_a + \dot{\theta}_a - \omega_s, \tag{21}$$

$$u_2 \stackrel{\Delta}{=} \boldsymbol{g}_2^{*T} \boldsymbol{H}^* \quad \Rightarrow \quad u_2 = H_2 \cos\theta + H_3 \sin\theta, \tag{22}$$

where (21) takes into account the input-additive disturbing component ω_s, and (22) includes the longitudinal and lateral skid-slip components v_{sxg} and v_{syg}. Since (21) depends on h_1 defined in (17), the *orienting role* played by the input u_1 in the overall control process becomes evident. On the other hand, definition (22) satisfies the heuristic concept of *careful pushing* mentioned in Subsection 3.1. Moreover, it can be shown that (22) guarantees convergence given by (12) also in the sense of the norms of vectors $\dot{\boldsymbol{q}}^*$ and $\boldsymbol{h}^*$.

The VFO control strategy with the skid-slip influence compensation has been graphically illustrated in Fig. 2 for two cases: where the relation (12) is perfectly satisfied: $\dot{\boldsymbol{q}}^* - \boldsymbol{h}^* = \boldsymbol{0}$ (case B), and where the relation (12) is under realization (case A).

We can now formulate the following proposition.

Proposition 1 *Assuming that:*

A1. the admissible reference trajectory $\boldsymbol{q}_t(\tau)$ satisfies (6) and is sufficiently smooth so that: $\dot{\theta}_t(\tau), \dot{\boldsymbol{q}}_t^*(\tau), \ddot{\boldsymbol{q}}_t^*(\tau) \in \mathcal{L}_\infty$,

A2. skid-slip components satisfy (7) and (8),

A3. $\forall_{\tau \geqslant 0}\ \boldsymbol{H}^*(\tau) \neq \boldsymbol{0}$

the VFO control law with skid-slip influence compensation proposed in (21)-(22) applied to system (4) solves Problem 1.

Proof. Let us first consider behavior of the auxiliary error (16). Substituting (21) into (4) yields the equation $\dot{e}_a + k_1 e_a = 0$, which clearly implies boundedness and exponential convergence of e_a to zero:

$$e_a(\tau) \in \mathcal{L}_\infty, \qquad \lim_{\tau\to\infty} e_a(\tau) = 0. \tag{23}$$

In a second stage we consider the time-evolution of the position error $\boldsymbol{e}^* = [e_x \ e_y]^T$. From (10), (11), and (14) one can write

$$\dot{\boldsymbol{e}}^* = -k_p \boldsymbol{e}^* + \boldsymbol{r}, \qquad \boldsymbol{r} \triangleq \boldsymbol{H}^* - \boldsymbol{g}_2^* u_2, \tag{24}$$

where $\boldsymbol{H}^* = k_p \boldsymbol{e}^* + \dot{\boldsymbol{q}}_t^* - \boldsymbol{v}_{sg}^*$. Moreover, it can be shown (see Appendix) that the following expressions are true:

$$\| \boldsymbol{r} \| = \| \boldsymbol{H}^* \| \, \gamma(\theta) \qquad \text{and} \qquad \lim_{\theta\to\theta_a} \gamma(\theta) = 0, \tag{25}$$

where $\gamma(\theta) = \sqrt{1 - \cos^2 \alpha(\theta)} \in [0, 1]$ and $\alpha(\theta) = \angle(\boldsymbol{g}_2^*(\theta), \boldsymbol{H}^*)$. The subsequent analysis will utilize considerations and lemmas included in [7] related to stability of perturbed systems (pages 350–355). Following the mentioned reference, let us treat (24) as a nominal system

$$\dot{\boldsymbol{e}}^* = \boldsymbol{f}(\boldsymbol{e}^*), \qquad \boldsymbol{f}(\boldsymbol{e}^*) = -k_p \boldsymbol{e}^* \tag{26}$$

with the perturbation $\boldsymbol{r} = \boldsymbol{r}(\boldsymbol{e}^*) = \boldsymbol{H}^*(\boldsymbol{e}^*, \dot{\boldsymbol{q}}_t^*, \boldsymbol{v}_{sg}^*) - \boldsymbol{g}_2^* u_2$. Recalling that $\boldsymbol{H}^* = k_p \boldsymbol{e}^* + \dot{\boldsymbol{q}}_t^* - \boldsymbol{v}_{sg}^*$ the upper bound of the perturbation can be assessed as follows:

$$\forall_{\tau \geqslant 0,\, \boldsymbol{e}^* \in \mathbb{R}^2} \ \| \boldsymbol{r}(\boldsymbol{e}^*) \| \ \leqslant \ \gamma'(\tau) \, \| \boldsymbol{e}^* \| + \Delta(\tau),$$

where $\gamma'(\tau) = k_p \gamma(\tau)$ and $\Delta(\tau) = \gamma(\tau) \left\| \dot{\boldsymbol{q}}_t^*(\tau) + \boldsymbol{v}_{sg}^*(\tau) \right\|$. Note, that $\gamma'(\tau)$ and $\Delta(\tau)$ are nonnegative, bounded and continuous (assumptions A1 and A2). Moreover, since $\lim_{\tau\to\infty} \gamma(\tau) = 0$ also $\gamma'(\tau) \to 0$ and $\Delta(\tau) \to 0$ for $\tau \to \infty$. It is evident that $V \triangleq \frac{1}{2} \boldsymbol{e}^{*T} \boldsymbol{e}^*$ is a Lyapunov function for the nominal system (26), since for all $\tau \geqslant 0$ and for all $\boldsymbol{e}^* \in \mathbb{R}^2$ the following inequalities hold: $c_1 \| \boldsymbol{e}^* \|^2 \leqslant V(\boldsymbol{e}^*) \leqslant c_2 \| \boldsymbol{e}^* \|^2$, $\frac{\partial V}{\partial \boldsymbol{e}^*} \boldsymbol{f}(\boldsymbol{e}^*) \leqslant -c_3 \| \boldsymbol{e}^* \|^2$ and $\left\| \frac{\partial V}{\partial \boldsymbol{e}^*} \right\| \leqslant c_4 \| \boldsymbol{e}^* \|$ with $c_1 = c_2 = 0.5$, $c_3 = k_p$ and $c_4 = 1$. As a consequence, $\boldsymbol{e}^* = \boldsymbol{0}$ is an exponentially stable equilibrium point of the nominal system (26). Additionally, note that $\gamma'(\tau)$ satisfies the following condition (see [7] – eqs. (9.20,9.21) and Lemma 9.5): $\int_0^\tau \gamma'(\xi) d\xi \ \leqslant \ \varepsilon\tau + \eta$ for some nonnegative (and bounded) constants η and $\varepsilon < \frac{c_1 c_3}{c_2 c_4} = k_p$. Now, recalling Lemma 9.4 from [7] one concludes, that the solution $\boldsymbol{e}^*(\tau)$ of the perturbed system (24) satisfies the following inequality:

$$\| \boldsymbol{e}^*(\tau) \| \ \leqslant \ \rho \, \| \boldsymbol{e}^*(0) \| \, e^{-a\tau} + \rho \int_0^\tau e^{-a(\tau-\xi)} \Delta(\xi) d\xi \tag{27}$$

for $\boldsymbol{e}^*(0) \in \mathbb{R}^2$ and any bounded $\Delta(\tau)$, with $\rho = e^\eta \geqslant 1$, $a = (k_p - \varepsilon) > 0$. Moreover, according to Lemma 9.6 from [7], since $\lim_{\tau\to\infty} \Delta(\tau) = 0$, the solution $\boldsymbol{e}^*(\tau)$ of (24) asymptotically converges to zero: $\lim_{\tau\to\infty} \boldsymbol{e}^*(\tau) = \boldsymbol{0}$.

In the last step the boundedness of the orientation error e_θ can be concluded using the following reasoning. Using the model structure (1) and Fig. 1 one can write: $\theta = \arg(u_2 \boldsymbol{g}_2^*)$ and $\delta_s = \arg(\dot{\boldsymbol{q}}^*) - \theta$. Since at the limit for $\tau \to \infty$ one has $\theta = \theta_a$ and $\| \boldsymbol{e}^* \| = 0$ one concludes from (11) that for $\tau \to \infty$ hold: $\boldsymbol{h}^* = \dot{\boldsymbol{q}}_t^*$ and $\dot{\boldsymbol{q}}^* = \boldsymbol{h}^* = \dot{\boldsymbol{q}}_t^*$. Following further this way we obtain for $\tau \to \infty$: $\delta_s = \arg(\boldsymbol{h}^*) - \theta = \arg(\dot{\boldsymbol{q}}_t^*) - \theta = \theta_t - \theta = e_\theta$ (at least in $\mathbb{S}^1$). The latter conclusion stays in agreement with Theorem 4 presented in [20]. Now, using (7) together with the result from (23) one can conclude boundedness of e_θ.

Recalling definitions (21)-(22) one can claim what follows: since $\boldsymbol{e}^* \in \mathcal{L}_\infty$ (due to (27)) and $\dot{\boldsymbol{q}}_t^*, \boldsymbol{v}_{sg}^* \in \mathcal{L}_\infty$ (by assumption A1 and condition (7)) also $H_2, H_3 \in \mathcal{L}_\infty$ and in a consequence $u_2 \in \mathcal{L}_\infty$. From condition (7) and since $\dot{\boldsymbol{q}}_t^*, \ddot{\boldsymbol{q}}_t^*, \dot{\boldsymbol{v}}_{sg}^* \in \mathcal{L}_\infty$ (by assumption A1 and condition (8)) we have $\dot{\theta}_a \in \mathcal{L}_\infty$, what together with boundedness of e_a (due to (23)), boundedness of ω_s (from condition (7)) and boundedness of u_2 (shown above) yields $u_1 \in \mathcal{L}_\infty$.

□

Remark 2 *Relaxing assumption A3 to:* $\boldsymbol{H}^* \neq \boldsymbol{0}$ for almost all $\tau \geqslant 0$, *which means that* $\boldsymbol{H}^*$ *can temporarily degenerate to zero but it does not get stuck there, makes the control input (21) a discontinuous function. Discontinuity results from definition (15) and equation (18), which are not determined for* $\boldsymbol{H}^* = \boldsymbol{0}$. *Recalling that* $\boldsymbol{H}^* \triangleq \boldsymbol{h}^* - \boldsymbol{v}_{sg}^* = k_p \boldsymbol{e}^* + \dot{\boldsymbol{q}}_t^* - \boldsymbol{v}_{sg}^*$, *one can find that* $\boldsymbol{H}^* = \boldsymbol{0}$ *is related to two cases:*

C1. $\boldsymbol{e}^* \neq \boldsymbol{0} \wedge \boldsymbol{v}_{sg}^* = \boldsymbol{h}^* \Rightarrow$ *it may hold only during a transient stage,*

C2. $\boldsymbol{e}^* = \boldsymbol{0} \wedge \boldsymbol{v}_{sg}^* = \dot{\boldsymbol{q}}_t^* \Rightarrow$ *when a closed-loop system evolves exactly along* $\boldsymbol{q}_t^*$.

Since for $\boldsymbol{H}^* = \boldsymbol{0}$ *also* $u_2 = 0$ *(see (22)), the only term which in both cases drives a subsystem* $\dot{\boldsymbol{q}}^* = \boldsymbol{g}_2^* u_2 + \boldsymbol{v}_{sg}^*$ *is the skid velocity* $\boldsymbol{v}_{sg}^*$. *Hence, C1 describes the situation when the skid velocity* $\boldsymbol{v}_{sg}^*$ *drives the system toward*[7] $\boldsymbol{q}_t^*$, *and C2 relates to the situation when* $\boldsymbol{v}_{sg}^*$ *drives the system exactly along* $\boldsymbol{q}_t^*$. *Moreover, for C1 it can be seen from (25) that* $\boldsymbol{H}^* = \boldsymbol{0}$ *implies:* $\boldsymbol{r} = \boldsymbol{0} \Rightarrow \dot{\boldsymbol{e}}^* + k_p \boldsymbol{e}^* = \boldsymbol{0}$. *As a consequence, the boundedness and convergence of* $\boldsymbol{e}^*$ *are preserved. The two cases determine a discontinuity set of input* u_1, *but they seem to be non-attractive, non-persistent, and unlikely in practice. However, to get a well-defined control* u_1, *one can introduce additional definitions for* θ_a *and* $\dot{\theta}_a$ *in the assumed sufficiently small* ϵ*-vicinity of* $\boldsymbol{H}^* = \boldsymbol{0}$. *One proposes to take:*

$$\theta_a \triangleq \theta_a(\tau_-) \quad \textit{and} \quad \dot{\theta}_a \triangleq 0 \qquad \textit{for} \quad \| \boldsymbol{H}^* \| \leqslant \epsilon, \tag{28}$$

where $0 < \epsilon < \inf_\tau \left\| \dot{\boldsymbol{q}}_t^*(\tau) - \boldsymbol{v}_{sg}^*(\tau) \right\|$ *and* τ_- *denotes the time instant of reaching the* ϵ*-vicinity. Definitions (28) together with (15) allow the control function (21) to remain unchanged.*

Note, that the proposed control law (21)-(22) compensates the skid-slip influence in a nonlinear feed-forward manner using the skid-slip velocity and acceleration *measurements*. Hence, in the absence of the skid-slip phenomena the VFO control law (21)-(22) can be used without changes (using only zero values for the skid-slip velocity components v_{sxg}, v_{syg} and ω_s) to ensure asymptotic posture tracking for the vehicle (1) in the *nominal* case. Definitions (21)-(22) describe in this case the *nominal* VFO tracking controller proposed in [6].

Recalling (14), (19), (20) and (21) we can see that the skid-slip velocities as well as their time derivatives are involved in the proposed VFO control law computations. It is a serious challenge to obtain sufficiently good estimates of these signals in practical (*field*) conditions. Since there are no sensors directly measuring the skid-slip effects, we have to assess them indirectly from available measurements. Using the model structure (4) one can compute the skid-slip velocities as follows:

$$\omega_s = \dot{\theta} - u_1, \quad v_{sxg} = \dot{x} - u_2 \mathrm{c}\theta, \quad v_{syg} = \dot{y} - u_2 \mathrm{s}\theta, \tag{29}$$

[7] Note that $\boldsymbol{h}^*$ defines an instantaneous convergence direction.

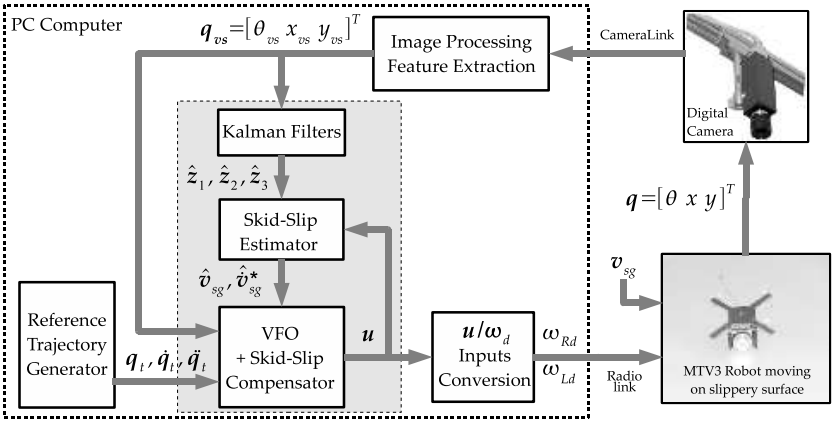

Figure 3: Block scheme of the VFO control system with skid-slip compensation

where $\mathrm{c}\theta \equiv \cos\theta$, $\mathrm{s}\theta \equiv \sin\theta$, and u_1, u_2 result from the proposed VFO control action. Differentiating v_{sxg} and v_{syg} with respect to time gives the following theoretical formulas for time-derivatives of skid-slip velocities:

$$\dot{v}_{sxg} = \ddot{x} + u_2\dot{\theta}\mathrm{s}\theta - \dot{u}_2\mathrm{c}\theta, \quad \dot{v}_{syg} = \ddot{y} - u_2\dot{\theta}\mathrm{c}\theta - \dot{u}_2\mathrm{s}\theta. \tag{30}$$

Utilization of formulas (29) and (30) in practice involves estimation of the terms $\dot{x}, \dot{y}, \dot{\theta}, \ddot{x}, \ddot{y}$ and $\dot{u}_2$. The time-derivatives of state variables have to be measured/estimated using the skid/slip-insensitive sensory systems like a vision cameras, gyroscopes, accelerometers, GPS etc. (positive results illustrating practical utilization of the mentioned sensors for vehicle localization and the state-derivatives and skid-slip estimation can be found in [8, 13, 19]). The latter term, $\dot{u}_2$, can be computed numerically using either the finite difference approximation (possibly filtered) or the so called *robust exact differentiator* introduced in [10]. Technical details of the skid-slip estimation algorithm used during conducted experiments are presented in the next section.

4 Experimental verification

4.1 Experimental setup

The experimental testbed consists of the differentially-DC motor-driven wheeled mobile robot MTV3 (presented in Fig. 4) moving on a slippery (teflon-like) surface, the monochrome digital vision camera SVS084MSCL used as an exteroceptive sensor measuring the vehicle's posture components (vision feedback), a PC-station realizing all high-level computations and a radio-transmission module allowing one to send the current command signals of the platform wheel velocities to two PI regulation loops implemented on a vehicle board. Selected technical parameters of the MTV3 robot are as follows: mass $m = 0.5$kg, wheel-base $b = 0.066$m, wheel radius $r = 0.026$m. High-level control loop with the VFO controller has been implemented with a sampling time $T = 0.022\,$s. The mobile robot was equipped with three LED markers mounted on the vehicle top. The vision system estimates the current vehicle posture utilizing LED markers of the robot. All needed computational blocks along with the skid-slip estimator and the VFO controller with the skid-slip compensator have been implemented in C/C++ language on a PC computer. Block scheme of the overall high-level control system has been illustrated in Fig. 3.

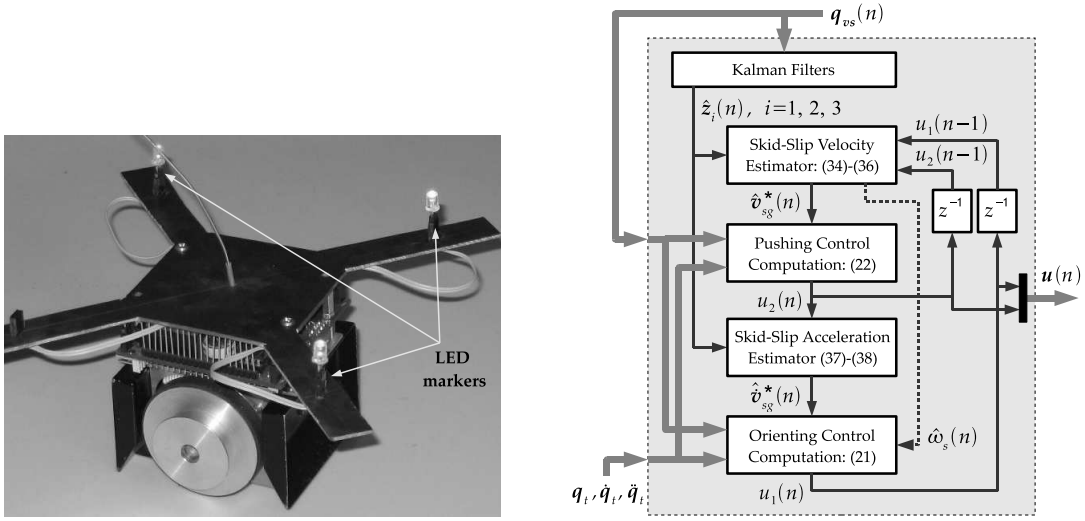

Figure 4: Differentially-driven mobile robot MTV3 (left) and the computation diagram of the VFO control law with skid-slip compensation (right)

4.2 Practical estimation of skid-slip velocities

Practical implementation of the skid-slip compensator involves efficient estimation of skid-slip velocities. Since vision feedback signals $\boldsymbol{q}_{vs} = [\theta_{vs}\ x_{vs}\ y_{vs}]^T$ are corrupted by measurement noise, the Kalman filter has been implemented to provide sufficiently smooth estimates of real velocity and acceleration components of the moving robot platform. For modeling purposes needed in Kalman filtering we defined three independent third-order discrete-time kinematic models describing the robot platform motion in all possible three degrees of freedom: one for angular and two for translational motions (see [1]). All models are represented by the following state and output equations:

$$\boldsymbol{z}_i\,(n+1) = \boldsymbol{A}\boldsymbol{z}_i\,(n) + \boldsymbol{w}_i(n), \tag{31}$$

$$y_i\,(n) = \boldsymbol{C}\boldsymbol{z}_i\,(n) + \varepsilon_i(n) \tag{32}$$

taking (for a sampling time T)

$$\boldsymbol{z}_i = \begin{bmatrix} z_{iq} \\ z_{iv} \\ z_{ia} \end{bmatrix}, \quad \boldsymbol{A} = \begin{bmatrix} 1 & T & 0 \\ 0 & 1 & T \\ 0 & 0 & 1 \end{bmatrix}, \quad \boldsymbol{C} = [1\ 0\ 0] \tag{33}$$

where z_{iq}, z_{iv}, z_{ia} denote respectively displacement, velocity and acceleration components of the ith degree of freedom with $z_{1q} := \theta, z_{2q} := x, z_{3q} := y$. We assumed white and uncorrelated process and measurement noises $\boldsymbol{w}_i \sim \mathcal{N}(\boldsymbol{0}, \boldsymbol{W}_i)$, $\varepsilon_i \sim \mathcal{N}(0, \sigma^2_{yi})$, where $\boldsymbol{W}_i = E[\boldsymbol{w}_i \boldsymbol{w}_i^T] = \mathrm{diag}\{\sigma^2_{iq}, \sigma^2_{iv}, \sigma^2_{ia}\}$, $\sigma^2_{yi} = E[\varepsilon_i^2]$. Due to classical implementation of the filter (see [1]) we restrict ourself only to recalling the prediction and correction stage equations which for the i-th degree of freedom take the form:

$$\overline{\boldsymbol{z}}_i(n) = \boldsymbol{A}\hat{\boldsymbol{z}}_i(n-1)$$

$$\hat{\boldsymbol{z}}_i(n) = \overline{\boldsymbol{z}}_i(n) + \boldsymbol{K}_i(n)\left[y_i(n) - \boldsymbol{C}\overline{\boldsymbol{z}}_i(n)\right],$$

where $\boldsymbol{K}_i(n)$ is a Kalman filter gain, $\overline{\boldsymbol{z}}_i$ denotes the predicted state and $\hat{\boldsymbol{z}}_i$ the corrected state estimate. Appropriate components of the corrected state estimate have been used in the skid-slip estimation procedure according to the following formulas (compare (29)):

$$\hat{\omega}_s(n) = \delta_\omega \left[\hat{z}_{1v}(n) - u_1(n-1)\right], \tag{34}$$
$$\hat{v}_{sxg}(n) = \delta_x \left[\hat{z}_{2v}(n) - u_2(n-1)\cos\hat{z}_{1q}(n)\right], \tag{35}$$
$$\hat{v}_{syg}(n) = \delta_y \left[\hat{z}_{3v}(n) - u_2(n-1)\sin\hat{z}_{1q}(n)\right] \tag{36}$$

and for skid-slip accelerations (compare with (30))

$$\hat{\dot{v}}_{sxg}(n) = \delta_x \left[\hat{z}_{2a}(n) + u_2(n)\hat{z}_{1v}(n)\mathrm{s}\hat{z}_{1q}(n) - \dot{u}_2^F(n)\mathrm{c}\hat{z}_{1q}(n)\right] \tag{37}$$
$$\hat{\dot{v}}_{syg}(n) = \delta_y \left[\hat{z}_{3a}(n) - u_2(n)\hat{z}_{1v}(n)\mathrm{c}\hat{z}_{1q}(n) - \dot{u}_2^F(n)\mathrm{s}\hat{z}_{1q}(n)\right] \tag{38}$$

where $\mathrm{s}z \equiv \sin z, \mathrm{c}z \equiv \cos z$, and $\delta_\omega, \delta_x, \delta_y \in (0,1]$ are the scaling factors – design parameters of the skid-slip estimator. The term $\dot{u}_2^F$ has been implemented as the filtered finite backward difference of u_2 signal samples.
The scaling factors δ_ω, δ_x and δ_y used in (34)-(38) play an important role in the effective and careful skid-slip compensation in practice. One can interpret their introduction as the proposition how in a simple way take into account the cross-coupling effect between the kinematic control action and the skid-slip disturbance, which is not modeled by equation (4). Explanation of the mentioned cross-couplings comes from the fact that realizing too high wheel velocities of the controlled vehicle can simultaneously deepen the skid-slip phenomena. Thus, the scaling factors allow realizing the *cautious compensation* preventing the dangerous effect of the practical skid-slip overestimation leading in extremal conditions to the loss of control over a vehicle.

The order of computations of the overall proposed VFO control strategy has been illustrated with a diagram in Fig. 4.

4.3 Experimental results

Three experiments have been conducted for two circular (ExpA and ExpB) and one elliptical (ExpC) reference trajectories. Circular trajectories were generated according to the equations: $x_t(\tau) := r_t \cos\omega_t\tau, y_t(\tau) := r_t \sin\omega_t\tau$ where for ExpA: $r_t = 0.25$m, $\omega_t = 3.3$rad/s (*small circle*), and for ExpB: $r_t = 0.32$m, $\omega_t = 3$rad/s (*big circle*). The elliptical trajectory for ExpC was computed according to the formulas: $x_t(\tau) := r_{xt}\cos\omega_t\tau, y_t(\tau) := r_{yt}\sin\omega_t\tau$ for $r_{xt} = 0.5$m, $r_{yt} = 0.25$m, and $\omega_t = 2$rad/s. During the experiments parameter values have been chosen as follows: $k_1 = 2$, $k_p = 1$ (VFO controller parameters) and $\delta_\omega = 0.45$, $\delta_x = \delta_y = 0.4$ (*cautious-compensation* scaling factors) for both the circular trajectories and $\delta_\omega = 0.35$, $\delta_x = \delta_y = 0.3$ for the elliptical trajectory, respectively.

Experiments have been conducted according to the scenario in which the robot initially was controlled by the nominal VFO controller with the skid-slip compensator turned off. After obtaining the vehicle motion under stable and intensively affecting skid-slip conditions the automatic sequence of turn-on/turn-off operations was initiated by the PC computer. The sequence allows revealing the differences in tracking quality with and without the compensator. Obtained results together with the skid-slip estimation quality are illustrated in Figs. 5-13.

4.4 Comments to the results

Analyzing the time plots (A) in Figs. 5, 8, and 11 one can see the substantial improvement of position tracking quality (especially for the circular trajectories) within the time

intervals when the skid-slip influence compensator was activated (time intervals denoted with ON mark). Obtained non-asymptotic behavior of the tracking error is a consequence of all the practical conditions like the state measurement noises, the skid-slip estimation errors, unmodeled robot dynamics, limited bandwidth of the control system and the mentioned cross-coupling effect, which have not been explicitly treated in the conducted theoretical analysis. Plots (D) present the high-level (robot platform level) control signals u_1, u_2. One may find that the main control effort is connected with the orienting control u_1 while the pushing control u_2 reveals only small fluctuations near some average value. The plots of geometrical paths drawn by the vehicle for the two ON/OFF successive sequences indicate also corrections made by the compensation action in the sense of the motion area occupied by the vehicle. It may have an important practical meaning from motion safety point of view in the cluttered environment. The results on plots (B) confirm the claimed boundedness of the orientation error e_θ and theoretically predicted convergence of e_θ to the skid-slip angle, especially within the ON-intervals (the skid-slip angle has been computed as $\delta_s = \arctan(\hat{v}_{sy}/\hat{v}_{sx})$, where $\hat{v}_{sx}$ and $\hat{v}_{sy}$ are the estimates of the skid-slip velocity components expressed in the local robot frame).

We would like to stress that the proposed VFO control strategy does not prevent nor attenuate the skid-slip phenomena but it attenuates its negative influence on the position tracking quality. It is especially visible on plots in Figs. 5(C) and 8(C), where the lateral skid-slip estimate $\hat{v}_{sy}$, computed according to (38) and expressed in a local vehicle body frame, persistently reaches relatively high values during the overall control time horizon. In the considered cases the lateral skid results mainly from the centrifugal acceleration, which is persistently present during the vehicle motion (also when the skid-slip compensator is active). Comparing plots from Figs. 5(C) and 8(C) one can find the higher skid-slip intensity in the latter case (*big circle* trajectory).

Motion conditions in the case of elliptical reference trajectory are qualitatively somewhat different. The curvature of the reference trajectory is now time-varying. Thus the intensity of the lateral skid phenomenon resulting from the centrifugal acceleration is not uniform along the whole elliptical path. Its maximal intensity falls into the neighborhoods of the ellipse's foci. Since the vehicle goes through the neighborhoods quite fast, there is no much time for the control system to substantially compensate the skid influence before subsequent transition of the vehicle into the region of relatively smaller skid intensity. As a consequence, obtained efficiency of the skid-slip compensation is better for the constant-curvature (circular) trajectories than for the elliptical one, which may result from limited bandwidth of the closed-loop system.

For quantitative comparison of tracking performance obtained for all experiments within two subsequent ON/OFF compensation sequences, the time plots of the chosen quality functional are presented in Figs. 6-7, 9-10, and 12-13. The quality functional represents the average tracking error power (within a selected time interval) and has been defined as follows:

$$J(nT) \triangleq \frac{1}{(n-n_i)T} \sum_{j=n_i}^{n} \| \boldsymbol{e}^*(jT) \|^2 , \tag{39}$$

where nT is a discrete time, and n_iT denotes the initial time instant of the selected time interval. Values of two functionals J^{ON} and J^{OFF} have been computed for particular time intervals of any one ON/OFF sequence. The tracking quality improvement ratios

$$R_i \triangleq [1 - J_i^{\mathrm{ON}}(nT)/J_i^{\mathrm{OFF}}(nT)] \cdot 100\%, \qquad i = 1, 2$$

Table 1: Tracking quality improvement ratios obtained during the conducted experiments

Experiment	R_1 (first ON/OFF)	R_2 (second ON/OFF)
ExpA	72.5%	76.8%
ExpB	85.2%	72.0%
ExpC	65.6%	46.0%

obtained for the ith ON/OFF sequence (for all three experiments) and computed for nT taken from the ends of particular ON/OFF time intervals are presented in Tab. 1. For both cases of circular trajectories the skid-slip compensation has provided the tracking quality improvement over 70%. For the elliptical trajectory the improvement ratios are not less than 46%.

5 Conclusions

In the paper the VFO control strategy extended with the skid-slip influence compensation scheme has been presented and practically tested. The skid and slip phenomena have been treated solely on the kinematic level in a form of an additional velocity vector disturbing the nominal nonholonomic vehicle kinematics. The skid-slip influence compensator has been formulated as a nonlinear feed-forward block, which in the absence of skid-slip effects can be easily turned off yielding the *nominal* VFO tracking controller originally proposed in [6]. Convergence properties of a closed-loop system formally analyzed in the paper stay in consistency with the general theoretical considerations presented recently in [20]. Experimental tests for three different relatively fast reference trajectories have been conducted in the laboratory setup equipped with a vision feedback. The results obtained during experiments revealed substantial quality improvement in position trajectory tracking for a differentially-driven vehicle moving in the presence of persistently affecting skid-slip phenomena.

Appendix

To shorten subsequent formulas the following notation will be used: $\mathrm{s}\beta \equiv \sin\beta$, $\mathrm{c}\beta \equiv \cos\beta$.

Construction of the norm $\|\boldsymbol{r}\|$. Recalling (24) and since $u_2 = \boldsymbol{g}_2^{*T}\boldsymbol{H}^* \equiv \|\boldsymbol{H}^*\|\cos\alpha$, where $\alpha = \angle(\boldsymbol{g}_2^*, \boldsymbol{H}^*)$ we have:

$$\boldsymbol{r} = \boldsymbol{H}^* - \boldsymbol{g}_2^* u_2 = \begin{bmatrix} H_2 \\ H_3 \end{bmatrix} - \begin{bmatrix} u_2\mathrm{c}\theta \\ u_2\mathrm{s}\theta \end{bmatrix} = \|\boldsymbol{H}^*\| \begin{bmatrix} \frac{H_2}{\|\boldsymbol{H}^*\|} - \mathrm{c}\alpha\mathrm{c}\theta \\ \frac{H_3}{\|\boldsymbol{H}^*\|} - \mathrm{c}\alpha\mathrm{s}\theta \end{bmatrix}.$$

Hence, one can write:

$$\|\boldsymbol{r}\|^2 = \|\boldsymbol{H}^*\|^2 \left[\frac{H_2^2}{\|\boldsymbol{H}^*\|^2} - \frac{2H_2\mathrm{c}\alpha\mathrm{c}\theta}{\|\boldsymbol{H}^*\|} + \mathrm{c}^2\alpha\mathrm{c}^2\theta + \frac{H_3^2}{\|\boldsymbol{H}^*\|^2} - \frac{2H_3\mathrm{c}\alpha\mathrm{s}\theta}{\|\boldsymbol{H}^*\|} + \mathrm{c}^2\alpha\mathrm{s}^2\theta \right] =$$

$$= \|\boldsymbol{H}^*\|^2 \left[1 - 2\mathrm{c}\alpha\frac{\boldsymbol{g}_2^{*T}\boldsymbol{H}^*}{\|\boldsymbol{H}^*\|} + \mathrm{c}^2\alpha \right] = \|\boldsymbol{H}^*\|^2 \left(1 - 2\mathrm{c}^2\alpha + \mathrm{c}^2\alpha\right) = \|\boldsymbol{H}^*\|^2 \left(1 - \mathrm{c}^2\alpha\right)$$

and finally $\|\boldsymbol{r}\| = \|\boldsymbol{H}^*\|\sqrt{1 - \cos^2\alpha(\theta)} = \|\boldsymbol{H}^*\|\gamma(\theta)$, since $\alpha = \alpha(\theta) = \angle(\boldsymbol{g}_2^*(\theta), \boldsymbol{H}^*)$.

Convergence of function $\gamma(\theta)$. Since $\gamma(\theta) = \sqrt{1 - \cos^2 \alpha(\theta)}$, we obtain:

$$\gamma^2(\theta) = 1 - \cos^2 \alpha(\theta) = 1 - \frac{(H_2 \mathrm{c}\theta + H_3 \mathrm{s}\theta)^2}{\| \boldsymbol{H}^* \|^2 \, \| \boldsymbol{g}_2^*(\theta) \|^2} = \frac{(H_2 \mathrm{s}\theta - H_3 \mathrm{c}\theta)^2}{H_2^2 + H_3^2}.$$

Recalling (23) we have $\theta(\tau) \to \theta_a(\tau)$ for $\tau \to \infty$ and from (15) one can obtain: $\lim_{\theta \to \theta_a} \tan\theta = (H_3/H_2) \;\Rightarrow\; \lim_{\theta \to \theta_a} \sin\theta = (H_3 \cos\theta)/H_2$, which substituted into the preceding equation allows concluding: $\lim_{\theta \to \theta_a} \gamma(\theta) = 0$.

References

[1] Y. Bar-Shalom, X. R. Li, and T. Kirubarajan. *Estimation with Applications to Tracking and Navigation*. Wiley-Interscience, New York, 2001.

[2] M. L. Corradini, T. Leo, and G. Orlando. Robust stabilization of a mobile robot violating the nonholonomic constraint via quasi-sliding modes. In *Proceedings of the American Control Conference*, pages 3935–3939, San Diego, California, 1999.

[3] M. L. Corradini, T. Leo, and G. Orlando. Experimental testing of a discrete-time sliding mode controller for trajectory tracking of a wheeled mobile robot in the presence of skidding effects. *Journal of Robotic Systems*, 19(4):177–188, 2002.

[4] W. E. Dixon, D. M. Dawson, and E. Zergeroglu. Tracking and regulation control of a mobile robot system with kinematic disturbances: a variable structure-like approach. *Journal of Dynamic Systems, Measurement and Control*, 122:616–623, 2000.

[5] M. Michałek. VFO control for mobile vehicles in the presence of skid phenomenon. In *Robot Motion and Control 2007*, volume 360 of *Lecture Notes in Control and Information Sciences*, pages 57–66. Springer, 2007.

[6] M. Michałek and K. Kozłowski. Vector-Field-Orientation feedback control method for a differentially driven vehicle. *IEEE Transactions on Control Systems Technology*, 18(1):45–65, 2010.

[7] H. K. Khalil. *Nonlinear systems. 3rd Edition*. Prentice-Hall, Upper Saddle River, New Jersey, 2002.

[8] R. Lenain, B. Thuilot, C. Cariou, and P. Martinet. High accuracy path tracking for vehicles in presence of sliding: Application to farm vehicle automatic guidance for agricultural tasks. *Autonomuos Robots*, (21):79–97, 2006.

[9] W. Leroquais and B. d'Andrea-Novel. Modeling and control of wheeled mobile robots not satisfying ideal velocity constraints: the unicycle case. In *Proceedings of the 35th Conference on Decision and Control*, pages 1437–1442, Kobe, Japan, 1996.

[10] A. Levant. Robust exact differentiation via sliding mode technique. *Automatica*, 34(3):379–384, 1998.

[11] A. D. Lewis. When is a mechanical control system kinematic? In *Proceedings of the 38th Conference on Decision and Control*, pages 1162–1167, Phoenix, Arizona, USA, December 1999.

[12] D. Lhomme-Desages, Ch. Grand, and J-C. Guinot. Trajectory control of a four-wheel skid-steering vehicle over soft terrain using physical interaction model. In *Proceedings of the IEEE International Conference on Robotics and Automation*, pages 1164–1169, Roma, Italy, April 2007.

[13] C. B. Low and D. Wang. GPS-based path following control for a car-like wheeled mobile robot with skidding and slipping. *IEEE Transactions on Control Systems Technology*, 16(2):340–347, 2008.

[14] P. Lucibello and G. Oriolo. Robust stabilization via iterative state steering with an application to chained-form systems. *Automatica*, 37:71–79, 2001.

[15] J. L. Martínez, A. Mandow, J. Morales, S. Pedraza, and A. García-Cerezo. Approximating kinematics for tracked mobile robots. *The International Journal of Robotics Research*, 24(10):867–878, 2005.

[16] I. Motte and G. Campion. A slow manifold approach for the control of mobile robots not satisfying the kinematic constraints. *IEEE Transactions on Robotics and Automation*, 16(6):875–880, 2000.

[17] K. Kozłowski and D. Pazderski. Practical stabilization of a skid-steering mobile robot - a kinematic-based approach. In *IEEE International Conference on Mechatronics*, pages 519–524, Budapest, Hungary, 2006.

[18] D. Pazderski and K. Kozłowski. Trajectory tracking control of skid-steering robot – experimental validation. In *Proceedings of 17th IFAC World Congress*, pages 5377–5382, Seoul, Korea, 2008.

[19] D. Piyabongkarn, R. Rajamani, J. A. Grogg, and J. Y. Lew. Development and experimental evaluation of a slip angle estimator for vehicle stability control. *IEEE Transactions on Control Systems Technology*, 17(1):78–88, 2009.

[20] D. Wang and C. B. Low. Modeling and analysis of skidding and slipping in wheeled mobile robots: control design perspective. *IEEE Transactions on Robotics*, 24(3):676–687, 2008.

[21] J. Y. Wong. *Theory of Ground Vehicles*. John Wiley & Sons, Inc., Ottawa, Canada, 2001.

[22] Zibin Zong, Yahya H Zweiri, and Lakmal D. Seneviratne. Non-linear observer for slip estimation of skid-steering vehicles. In *Proceedings of the IEEE International Conference on Robotics and Automation*, pages 1499–1504, Orlando, Florida, USA, May 2006.

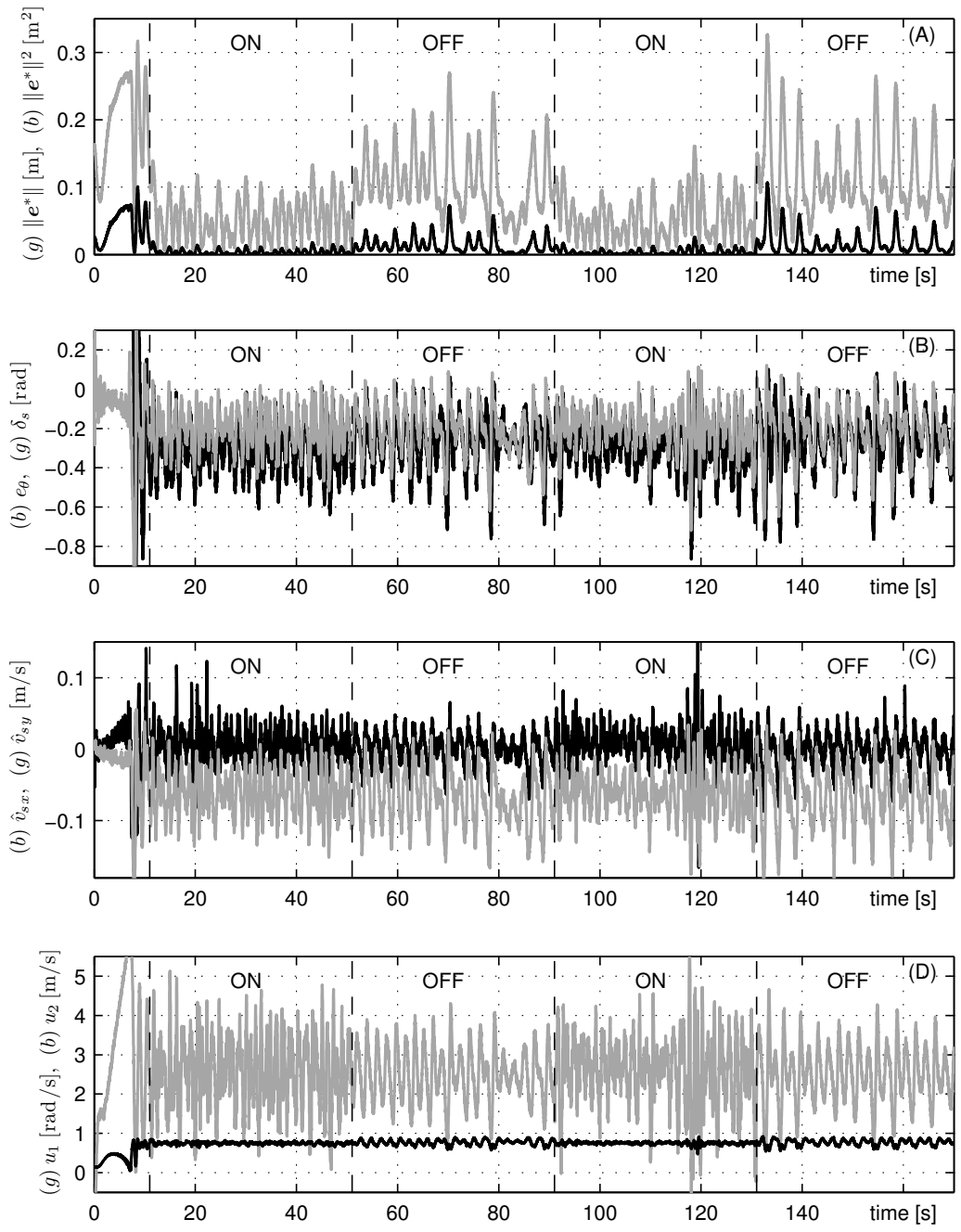

Figure 5: ExpA: Time plots of selected signals ((*b*)–black, (*g*)–gray) for the *small circle* trajectory

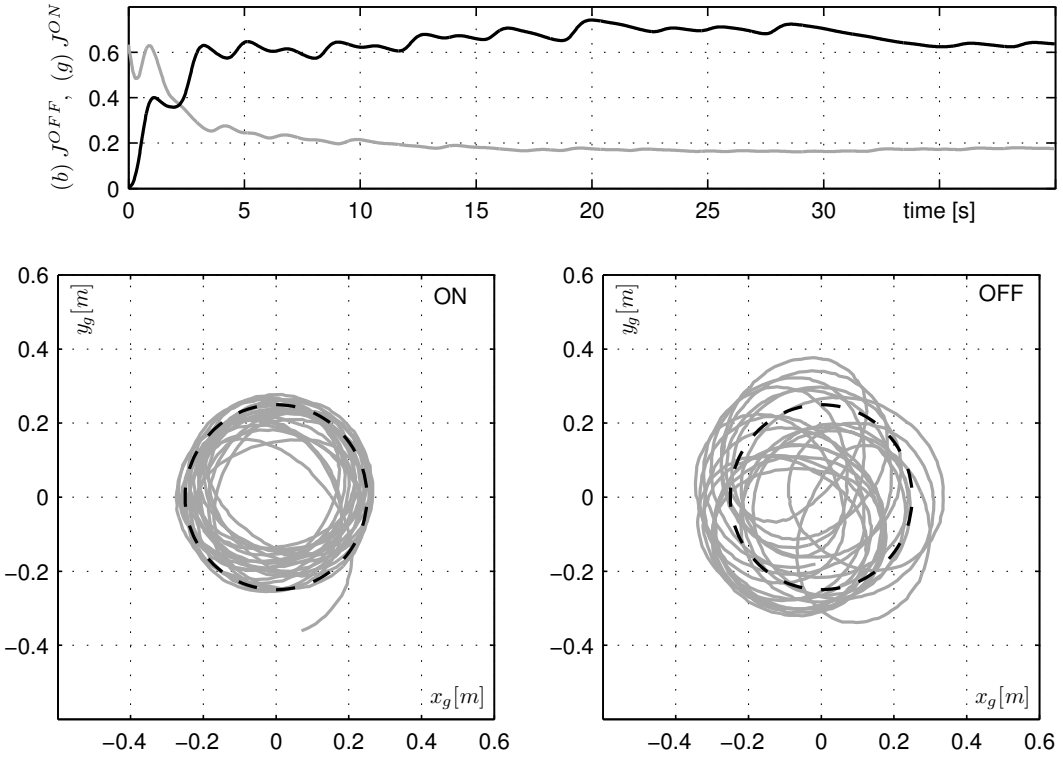

Figure 6: ExpA: Time plots of quality functionals and the geometrical paths drawn by the vehicle within the first ON/OFF compensation sequence (reference path denoted by the dashed line)

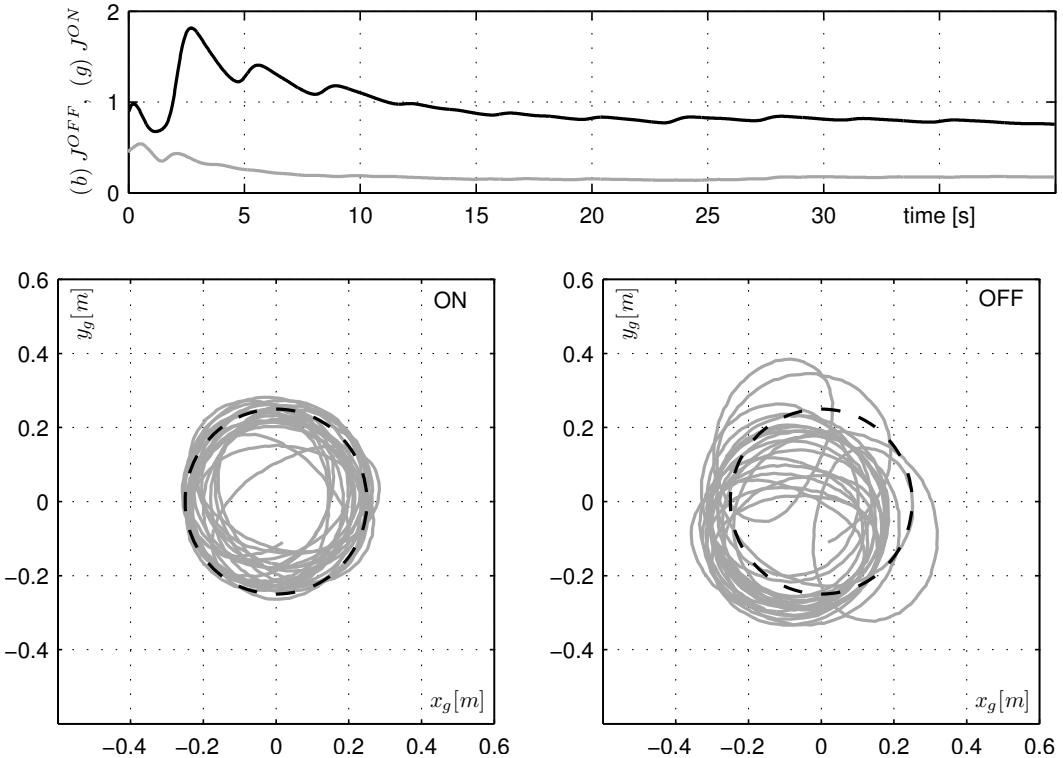

Figure 7: ExpA: Time plots of quality functionals and the geometrical paths drawn by the vehicle within the second ON/OFF compensation sequence (reference path denoted by the dashed line)

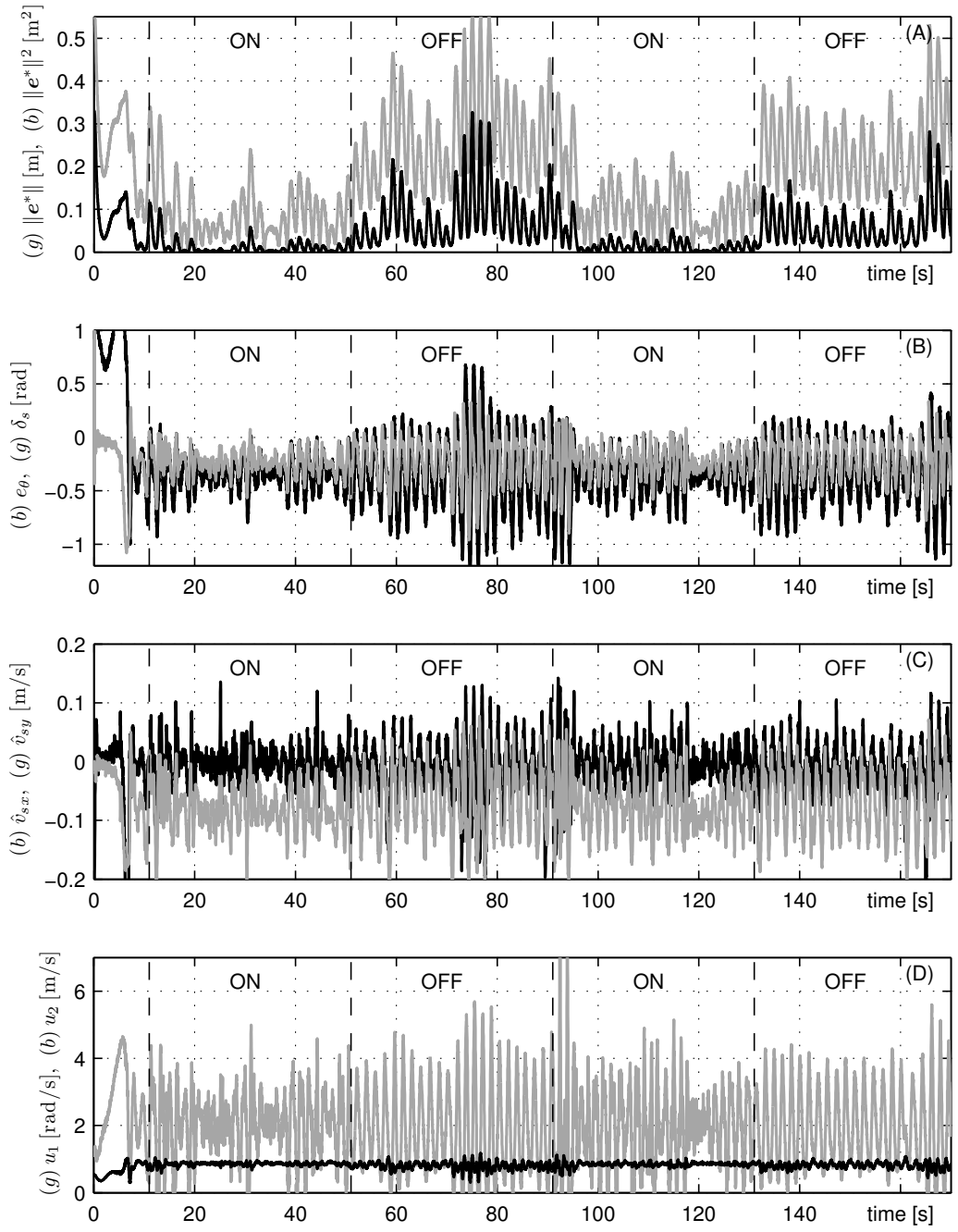

Figure 8: ExpB: Time plots of selected signals ((*b*)–black, (*g*)–gray) for the *big circle* trajectory

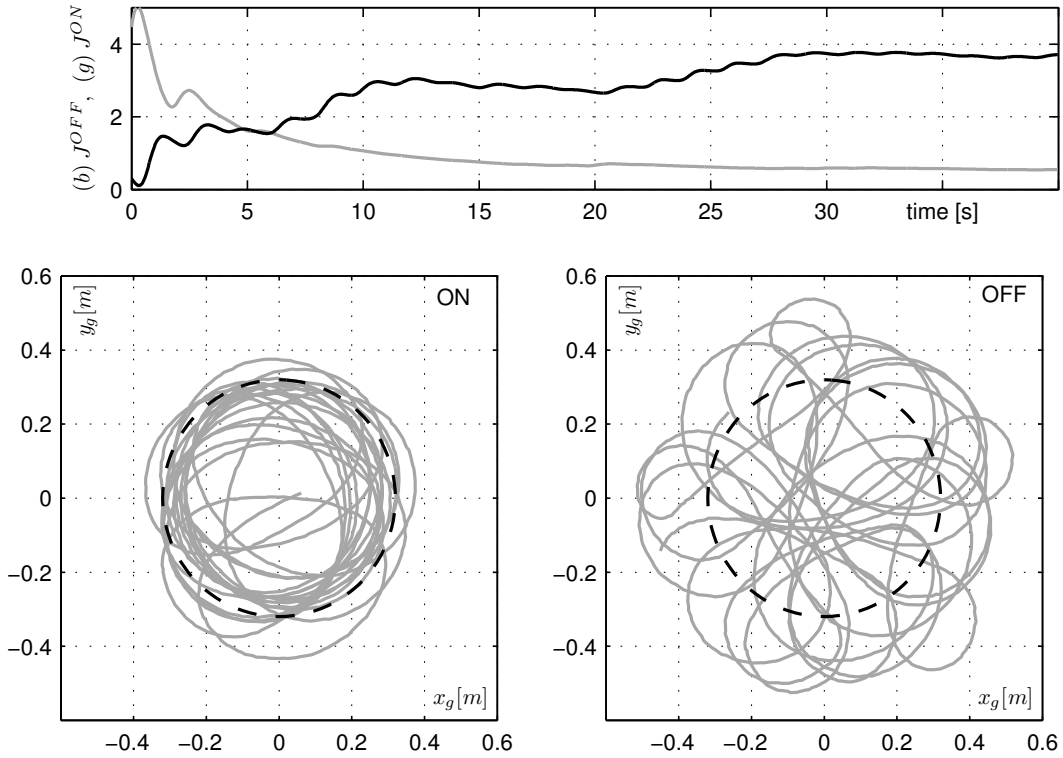

Figure 9: ExpB: Time plots of quality functionals and the geometrical paths drawn by the vehicle within the first ON/OFF compensation sequence (reference path denoted by the dashed line)

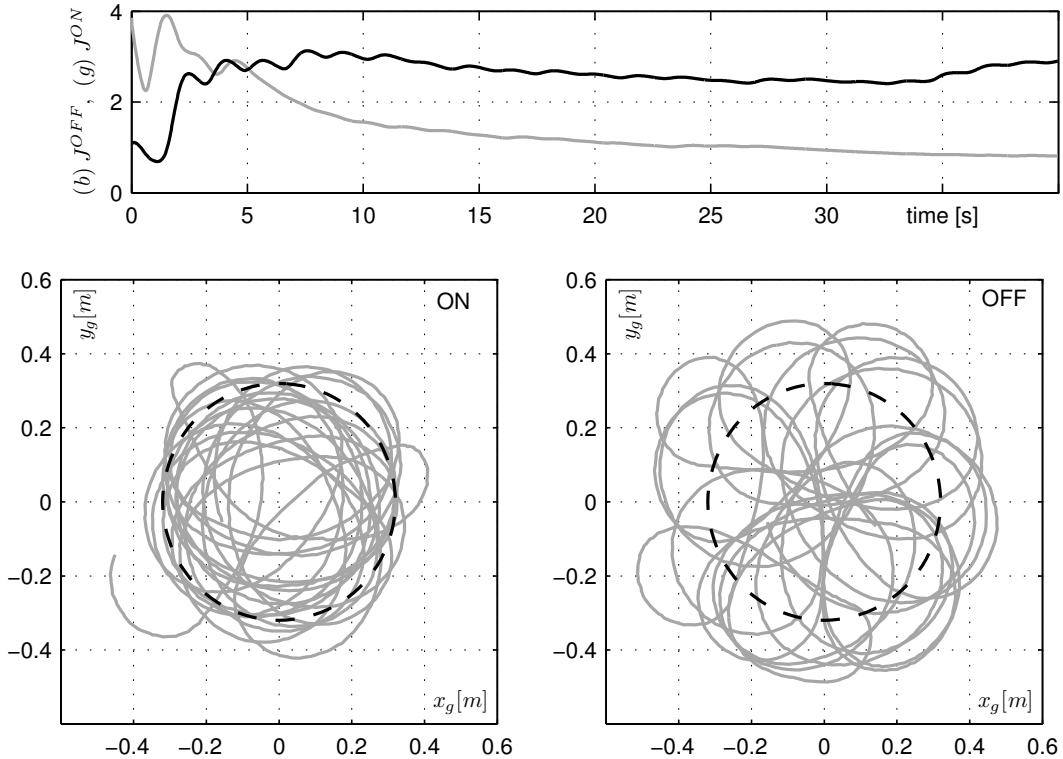

Figure 10: ExpB: Time plots of quality functionals and the geometrical paths drawn by the vehicle within the second ON/OFF compensation sequence (reference path denoted by the dashed line)

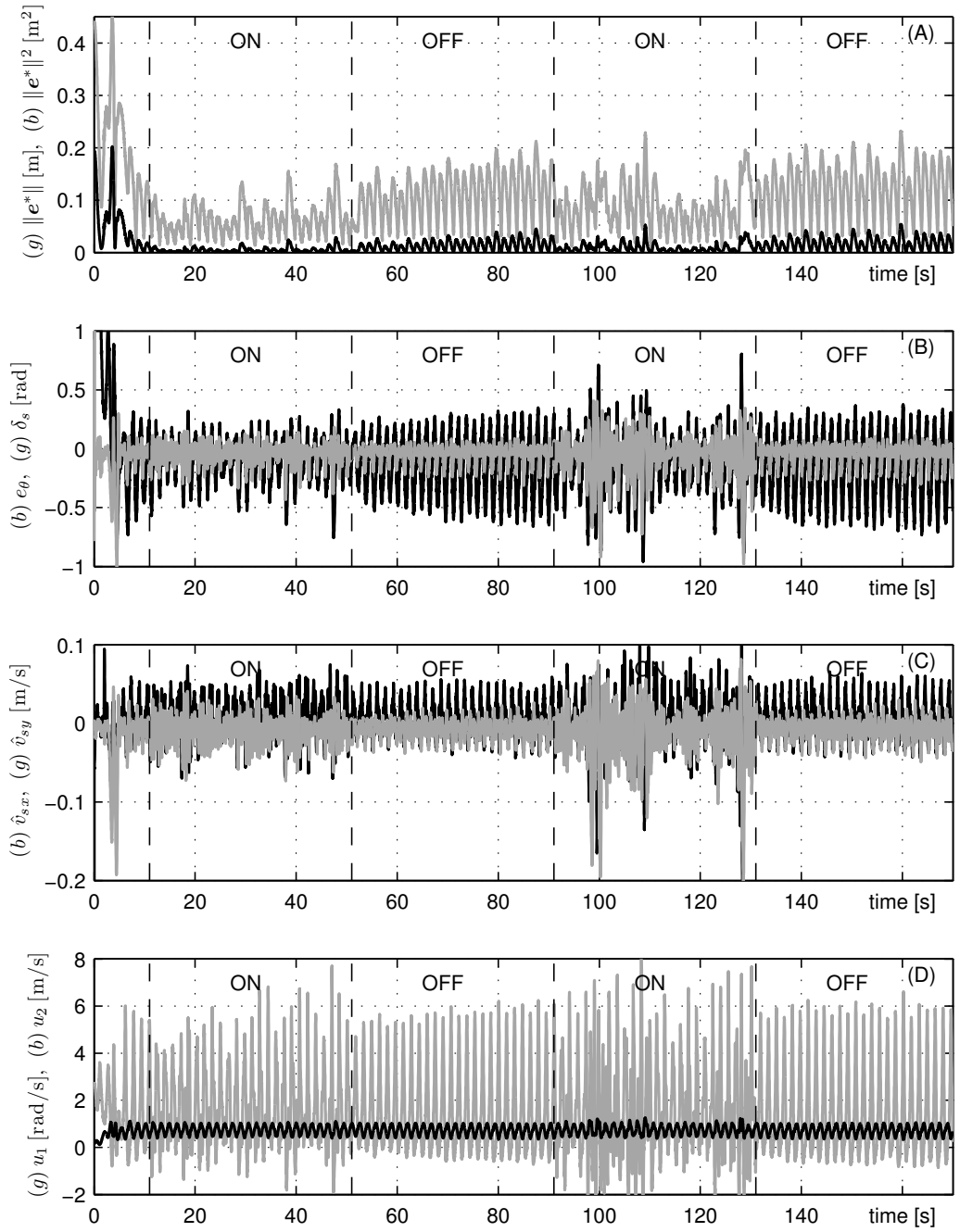

Figure 11: ExpC: Time plots of selected signals ((*b*)–black, (*g*)–gray) for the elliptical trajectory

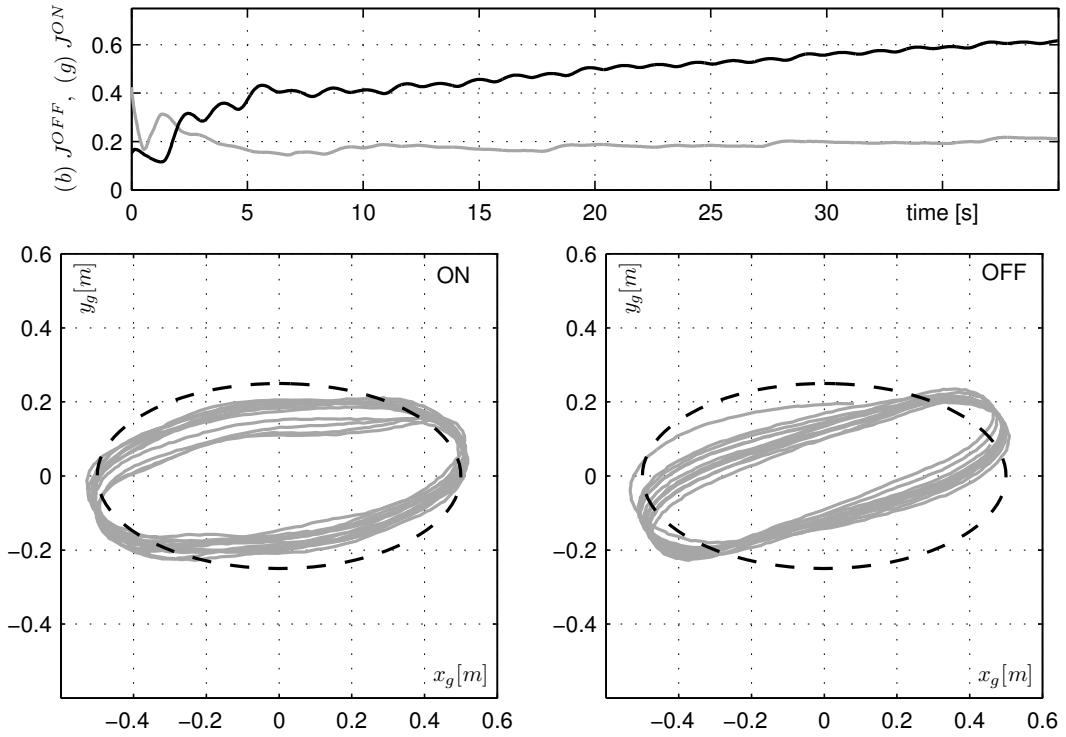

Figure 12: ExpC: Time plots of quality functionals and the geometrical paths drawn by the vehicle within the first ON/OFF compensation sequence (reference path denoted by the dashed line)

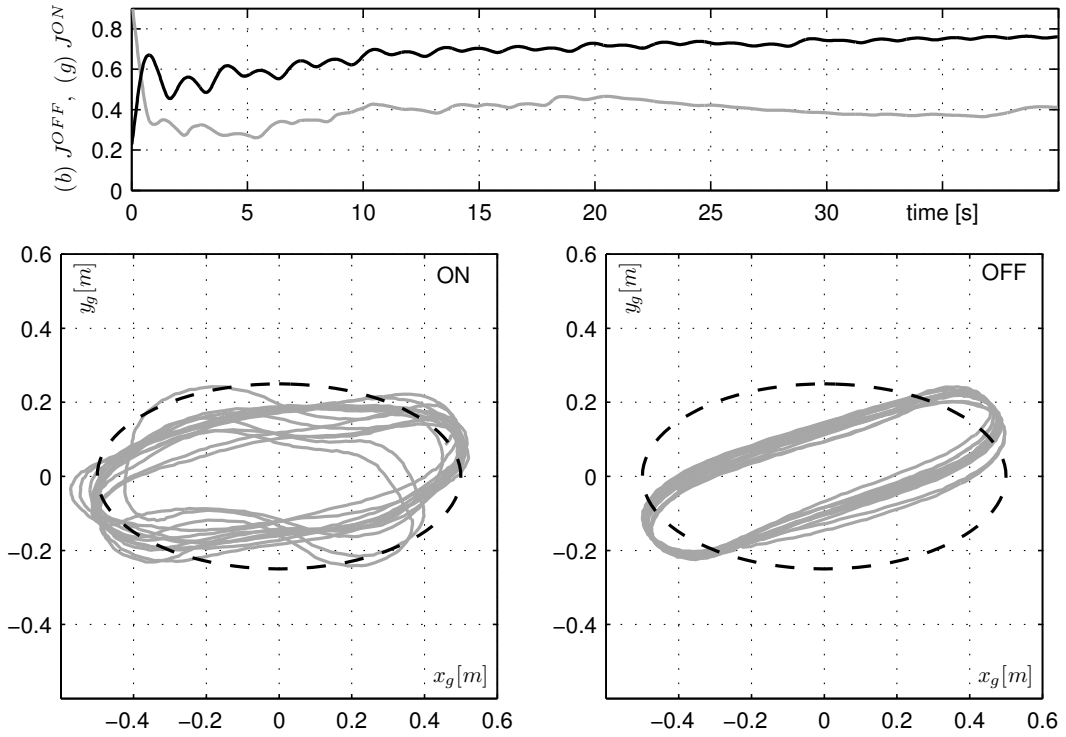

Figure 13: ExpC: Time plots of quality functionals and the geometrical paths drawn by the vehicle within the second ON/OFF compensation sequence (reference path denoted by the dashed line)